

Cyclization and Relaxation Dynamics of Finite-Length Collapsed Self-Avoiding Polymers

Julian Kappler,¹ Frank Noé,² and Roland R. Netz¹¹*Department of Physics, Freie Universität Berlin, 14195 Berlin, Germany*²*Department of Mathematics and Computer Science, Freie Universität Berlin, 14195 Berlin, Germany* (Received 21 June 2018; revised manuscript received 23 November 2018; published 12 February 2019)

We study the cyclization and relaxation dynamics of ideal as well as interacting polymers as a function of chain length N . For the cyclization time τ_{cyc} of ideal chains we recover the known scaling $\tau_{\text{cyc}} \sim N^2$ for different backbone models, for a self-avoiding slightly collapsed chain we obtain from Langevin simulations and scaling theory a modified scaling $\tau_{\text{cyc}} \sim N^{5/3}$. The cyclization and relaxation dynamics of a finite-length collapsed chain scale differently; this unexpected dynamic multiscale behavior is rationalized by the crossover between swollen and collapsed chain behavior.

DOI: 10.1103/PhysRevLett.122.067801

The loop formation kinetics of polymers governs the dynamics of protein folding [1–3] and gene expression regulation [4–7]. The quantity of main interest is the cyclization time τ_{cyc} , i.e., the mean time it takes the two polymer ends to reach a cyclization radius R_{cyc} for the first time after starting from a distance $R_s > R_{\text{cyc}}$. Pioneering theoretical works for Gaussian chains predicted τ_{cyc} to scale with the monomer number N as

$$\tau_{\text{cyc}} \sim N^\alpha, \quad (1)$$

with the Wilemski-Fixman (WF) scaling $\alpha = 2$ for intermediate R_{cyc} [8–11], and the Szabo-Schulten-Schulten (SSS) scaling $\alpha = 3/2$ for small R_{cyc} [12].

For ideal chains, without monomer-monomer interactions, the crossover and asymptotic scaling behavior has been studied both analytically [4,13–17] and numerically [18–20]. Experiments on short chains confirmed the SSS scaling $\alpha = 3/2$ [2,3,21]. Numerical [22–24] and experimental [25] studies of self-avoiding swollen chains find $\alpha \approx 2.2$, consistent with approximate analytical methods [24]. For the particularly interesting case of a self-avoiding collapsed chain, as relevant for the initial steps of protein folding, only few results exist [24,26–28], indicating $\alpha \approx 5/3$. Typically, theories and simulations use simplified polymeric backbone models, and it is not clear whether realistic backbone models with constrained bond lengths and bond angles modify τ_{cyc} .

In this work we consider the dynamics of the end-to-end distance R_{ete} of three different polymer backbone models, namely, the Gaussian (G), freely jointed (FJ), and freely rotating (FR) models; see Fig. 1. We furthermore consider an interacting Gaussian chain that includes Lennard-Jones interactions (GLJ). From Langevin simulations we extract cyclization times τ_{cyc} and recover for ideal chains, depending on the cyclization radius R_{cyc} , the WF and SSS scaling

laws, independent of the backbone model. However, for an interacting collapsed chain we find the asymptotic scaling $\tau_{\text{cyc}} \sim N^{5/3}$, in agreement with scaling predictions for a collapsed chain [28]. Thus, cyclization dynamics is insensitive to polymer backbone details but substantially influenced by nonbonded interactions. To relate these results to the dynamics of R_{ete} , which is a collective variable that involves all polymer degrees of freedom [4,15,17], we map the dynamics of R_{ete} onto the generalized Langevin equation (GLE) that accounts for non-Markovian effects via a memory kernel $\Gamma(t)$ [24,29–32]. We find that the memory kernels of all ideal chains considered decay as $\Gamma(t) \sim t^{-1/2}$ for intermediate times t , while for the interacting collapsed chain $\Gamma(t) \sim t^{-6/11}$, a scaling expected for a swollen rather than a collapsed chain. This demonstrates that the dynamics of a self-avoiding collapsed chain exhibits signatures of both collapsed and swollen chain behavior, reflecting the complex polymer relaxation kinetics observed in experiments [25].

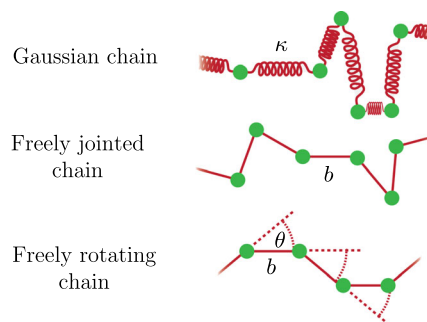


FIG. 1. Illustration of different backbone models considered. In the Gaussian model, neighboring monomers are bound by harmonic potentials. In the freely jointed model, the bond length b between neighboring monomers is constrained. In the freely rotating chain model both bond length b and bond angle θ are constrained.

We perform Langevin simulations at a temperature $T = 300$ K using the GROMACS 2016.3 simulation package [33] with parameters for alkane chains from the gromos53a6 forcefield [34]; see the Supplemental Material [35] for details. Friction coefficients approximate methane in water, masses are enhanced by a factor of 100, which improves the numerical accuracy of $\Gamma(t)$ without modifying the relevant long-time behavior. For the Gaussian chain model neighboring monomers are subject to a harmonic potential which produces a mean-squared distance $b^2 = 0.153^2$ nm². For the FJ model the distance between neighboring monomers is constrained to $b = 0.153$ nm, in the FR model in addition bond angles are constrained to $\theta = 111^\circ$. All these models are ideal, i.e., without nonbonded interactions. The GLJ model is based on the Gaussian chain model and includes the gromos53a6 Lennard-Jones (LJ) interactions for alkane chains [34], which produces a collapsed chain of self-avoiding segments that cannot cross each other [35].

We map our Langevin trajectories onto the GLE,

$$\mu \ddot{\mathbf{R}}_{\text{ete}}(t) = - \int_0^t dt' \Gamma(t-t') \dot{\mathbf{R}}_{\text{ete}}(t') - \nabla U[\mathbf{R}_{\text{ete}}(t)] + F_R(t), \quad (2)$$

where $R_{\text{ete}} = \sqrt{(\vec{\mathbf{R}}_{N-1} - \vec{\mathbf{R}}_0)^2}$ is the scalar end-to-end distance with $\vec{\mathbf{R}}_i$ the position of monomer i , μ is an effective mass, ∇U is the derivative of the effective potential $U(R_{\text{ete}})$, $\Gamma(t)$ is the memory kernel, and the random force $F_R(t)$ obeys the fluctuation-dissipation theorem $\langle F_R(t) F_R(t') \rangle = k_B T \Gamma(|t-t'|)$. We extract all parameters of the GLE from simulations [35–37].

Figure 2 compares memory kernels for the end-to-end distance vector, $\vec{\mathbf{R}}_{\text{ete}} = \vec{\mathbf{R}}_{N-1} - \vec{\mathbf{R}}_0$, extracted from simulations of Gaussian chains, to analytical predictions based on the Mori-Zwanzig projection formalism [38,39]; see Supplemental Material for details [35]. The perfect agreement validates our numerical method for extracting $\Gamma(t)$ from simulations also for the scalar end-to-end distance, for

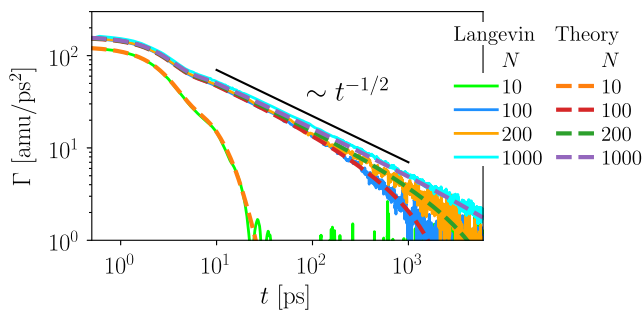


FIG. 2. Comparison of analytically and numerically calculated memory kernels for the end-to-end distance vector $\vec{\mathbf{R}}_{\text{ete}}$ of a Gaussian chain.

which no exact calculation is possible. For $N \gtrsim 100$, $\Gamma(t)$ shows an intermediate $\Gamma(t) \sim t^{-1/2}$ scaling regime, similar to recent results for the position of the central monomer of a Gaussian chain [29,31].

Figure 3(b) shows U as a function of R_{ete} rescaled by the (for the GLJ model N -dependent) Kuhn length a_i , which is defined by $\langle R_{\text{ete}}^2 \rangle \equiv a_i L$, where $i = G, FJ, FR, GLJ$ indicates the chain model, and $L = (N-1)b$ is the contour length. The potentials of all ideal chains are very similar. This is reflected by the mean squared end-to-end distance $\langle R_{\text{ete}}^2 \rangle$ in Fig. 3(c), where all ideal chains yield a linear scaling $\langle R_{\text{ete}}^2 \rangle = a_i b (N-1)$ with $a_G = a_{FJ} = b$, $a_{FR} = b \sqrt{(1 + \cos \theta)/(1 - \cos \theta)}$ [40], consistent with the static power-law scaling

$$\langle R_{\text{ete}}^2 \rangle \sim N^{2\nu_{\text{st}}}, \quad (3)$$

with the ideal-chain Flory exponent $\nu_{\text{st}} = 1/2$. For the GLJ chain we observe swollen behavior for $N \lesssim 30$ with an exponent $\nu_{\text{st}} > 1/2$ [40,41] and a broad crossover to collapsed behavior for $N \gtrsim 100$ with an exponent $\nu_{\text{st}} = 1/3$ [27,41,42] as indicated by a dotted line. This is expected, since our LJ parameters model a hydrophobic chain in water.

In Fig. 3(d) we show simulation results for the mean squared displacement (MSD) of R_{ete} , which for intermediate time displays a power law according to

$$\langle \Delta R_{\text{ete}}^2(t) \rangle \equiv \langle [R_{\text{ete}}(t) - R_{\text{ete}}(0)]^2 \rangle \sim t^\beta. \quad (4)$$

From the dynamic size scaling of a diffusing subchain of N_{sub} monomers, $\langle R_{\text{sub}} \rangle \sim N_{\text{sub}}^{\nu_{\text{dyn}}}$, the diffusion law for the MSD of the subchain position, $\langle R_{\text{sub}}^2 \rangle \sim D_{\text{sub}} t$, and the diffusivity of a freely draining chain, $D_{\text{sub}} \sim 1/N_{\text{sub}}$, one obtains $N_{\text{sub}}^{2\nu_{\text{dyn}}+1} \sim t$ and thus [40,43–45]

$$\beta = 2\nu_{\text{dyn}}/(1 + 2\nu_{\text{dyn}}). \quad (5)$$

Here, ν_{dyn} characterizes the dynamic chain size and only in the asymptotic long-time large-polymer length limit equals the static Flory exponent ν_{st} , as we will detail further below. For ideal chains with $\nu_{\text{dyn}} = 1/2$ one obtains $\beta = 1/2$, in agreement with simulation results for the ideal chains in Fig. 3(d). For the GLJ chain, the simulation results are consistent with an exponent $\beta = 6/11$ over two decades in time [43,44], which follows from Eq. (5) for the exponent of a swollen chain $\nu_{\text{dyn}} = 3/5$ [40,41], but not for the collapsed exponent $\nu_{\text{dyn}} = 1/3$ which would yield $\beta = 2/3$ (clearly inconsistent with the simulation data). We thus observe swollen scaling $\nu_{\text{dyn}} = 3/5$ for the MSD in Fig. 3(d), while $\langle R_{\text{ete}}^2 \rangle$ in Fig. 3(c) is characterized by collapsed scaling $\nu_{\text{st}} = 1/3$ for large N . This is rationalized by the fact that the internal mean monomer distance $\langle (\vec{\mathbf{R}}_0 - \vec{\mathbf{R}}_i)^2 \rangle$ in Fig. 3(e) indeed exhibits swollen scaling

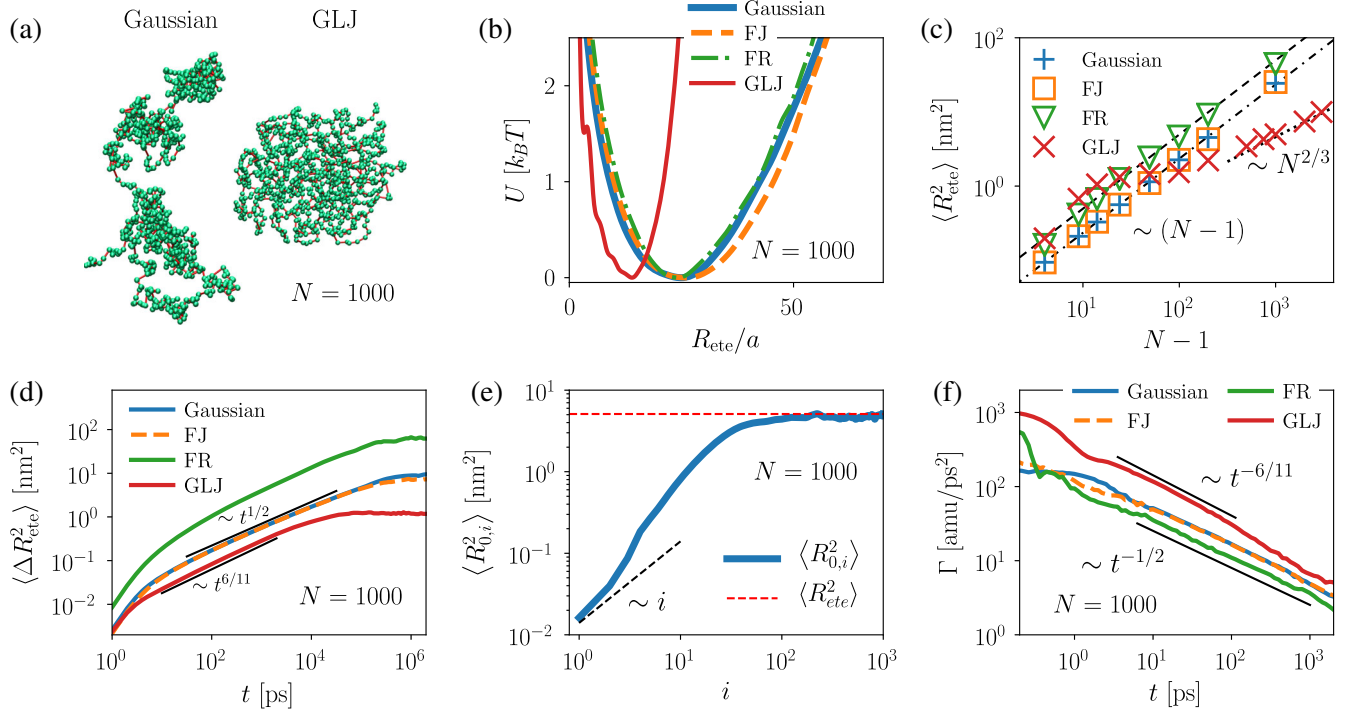


FIG. 3. (a) Simulation snapshots of Gaussian and GLJ chains. (b) Effective potential U for the end-to-end distance for $N = 1000$. (c) Mean squared end-to-end distance as a function of chain length N . Dashed and dash-dotted lines show predictions for FR and Gaussian/FJ chain models, respectively. The dotted line indicates the power law $\langle R_{\text{ete}}^2 \rangle \sim N^{2/3}$. (d) Mean-squared displacement of the end-to-end distance. For better visibility, the FR chain MSD is multiplied by 5. (e) Mean squared distance $\langle R_{0,i}^2 \rangle = \langle (\vec{R}_0 - \vec{R}_i)^2 \rangle$ between the terminal monomer and the i th monomer of a GLJ chain. The red dashed line represents the mean end-to-end distance $\langle R_{\text{ete}}^2 \rangle$. (f) Memory kernels for chain length $N = 1000$. The power laws indicated by black bars in (d) and (f) are justified by fits in the Supplemental Material [35].

with $\nu > 1/2$ on spatial scales for which the MSD in Fig. 3(d) is characterized by the swollen exponent $\beta = 6/11$.

To corroborate that the end-to-end distance dynamics is characterized by swollen chain statistics, we in Fig. 3(f) show memory kernels extracted from Langevin simulations for $N = 1000$. The kernel of the Gaussian chain scales as $\Gamma(t) \sim t^{-1/2}$ and, except for short times, agrees quantitatively with the FJ chain, demonstrating that the end-to-end dynamics is insensitive to details of the backbone model. This power law, which we also find for \bar{R}_{ete} in Fig. 2, reflects the Rouse spectrum [29,31]. Interestingly, Markov state models for the polymer dynamics show similar power-law distribution of timescales, see the Supplemental Material [35,46]. The kernel of the FR chain also scales as $\Gamma(t) \sim t^{-1/2}$ with a prefactor that results from the different Kuhn length, as detailed in the Supplemental Material [35]. The kernel of the GLJ chain exhibits a different power law, consistent with $\Gamma(t) \sim t^{-6/11}$ and in agreement with the expected relationship $\langle \Delta R_{\text{ete}}^2(t) \rangle \sim 1/\Gamma(t)$ [47], which is derived in the Supplemental Material [35]. We conclude that the dynamics of an interacting collapsed chain is at intermediate times, for which we can extract $\Gamma(t)$, characteristic of a swollen chain.

The cyclization time τ_{cyc} , defined in the introduction, is illustrated in the inset of Fig. 4(a), where we show $U(R_{\text{ete}})$ and τ_{cyc} for the GLJ model as a function of R_s for fixed $R_{\text{cyc}} = 3b \approx 0.46$ nm. For R_s not too close to R_{cyc} , τ_{cyc} is rather independent of R_s , so the scaling of τ_{cyc} should not critically depend on R_s , for which we use the minimum of U .

In Fig. 4(b) it is seen that τ_{cyc} exhibits power-law scaling according to Eq. (1). For ideal chains and rather large $R_{\text{cyc}} = 3b \approx 0.46$ nm, we obtain the ideal WF scaling $\alpha = 2$ [10]. This corresponds to the scaling of the chain relaxation time τ_{rel} and can be derived by equating the MSD, Eq. (4), with the equilibrium end-to-end radius, Eq. (3), leading to $\tau_{\text{rel}} \sim N^2$ with [28]

$$\lambda = 2\nu_{\text{st}}/\beta = \nu_{\text{st}}(2\nu_{\text{dyn}} + 1)/\nu_{\text{dyn}}, \quad (6)$$

where we used Eq. (5). For $\nu_{\text{st}} = \nu_{\text{dyn}} \equiv \nu$ this reduces to $\lambda = 2\nu + 1$ [48,49]. For an ideal chain with $\nu = 1/2$, and assuming that τ_{rel} and τ_{cyc} scale alike, we obtain the WF scaling $\alpha = \lambda = 2$ [10], as indeed observed for the ideal chains in Fig. 4(b).

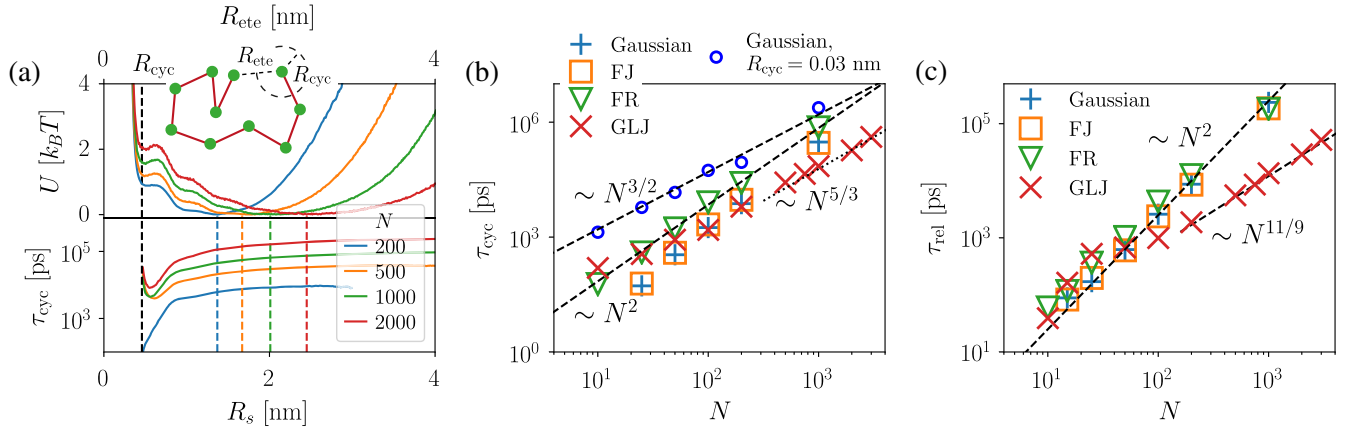


FIG. 4. (a) Effective potential U for the end-to-end distance of a GLJ chain as a function of R_{ete} (upper plot) and corresponding cyclization time τ_{cyc} (lower plot) as a function of the starting position R_s . The cyclization radius $R_{\text{cyc}} = 3b \approx 0.46$ nm is denoted by a black vertical dashed line; colored vertical dashed lines denote the respective positions of the minima of U . The inset illustrates the end-to-end distance R_{ete} and the cyclization radius R_{cyc} . (b) Cyclization time as a function of chain length N , together with scaling predictions indicated by lines. Except for the blue empty circles, where $R_{\text{cyc}} = 0.03$ nm, we use $R_{\text{cyc}} = 3b \approx 0.46$ nm. For R_s the minimum of U is used. (c) Chain relaxation time τ_{rel} (as defined in Fig. 5) as function of N .

For $R_{\text{cyc}} \ll \langle R_{\text{ete}} \rangle$ the cyclization time will eventually exceed τ_{rel} and cyclization becomes Markovian, in which limit τ_{cyc} is to leading order proportional to the inverse equilibrium probability for the two chain ends to be at the same position, thus $\tau_{\text{cyc}} \sim R_{\text{ete}}^3 \sim N^{3\nu_{\text{st}}}$ and

$$\alpha = 3\nu_{\text{st}}. \quad (7)$$

For an ideal chain, $\nu_{\text{st}} = 1/2$, we recover the SSS scaling $\tau_{\text{cyc}} \sim N^{3/2}$ [12], which indeed describes the simulation data in Fig. 4(b) for a small cyclization radius of $R_{\text{cyc}} = 0.03$ nm $\approx b/15$.

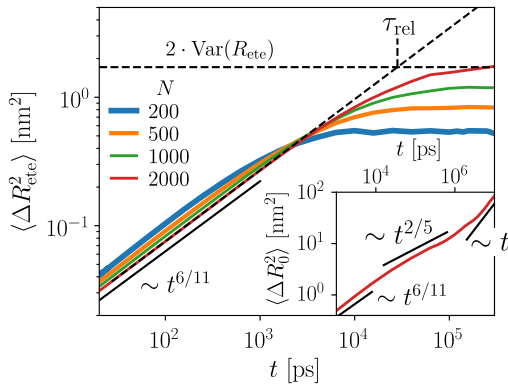


FIG. 5. The chain relaxation time τ_{rel} is defined by the intersect of the intermediate-time power-law behavior of $\langle \Delta R_{\text{ete}}^2(t) \rangle$ and the long-time limiting value $\lim_{t \rightarrow \infty} \langle \Delta R_{\text{ete}}^2(t) \rangle = 2\text{Var}(R_{\text{ete}})$ calculated directly from simulations. The dashed black lines illustrate the definition of τ_{rel} for $N = 2000$. The inset shows the MSD of a terminal monomer, $\langle \Delta R_0^2(t) \rangle = \langle [\vec{R}_0(t) - \vec{R}_0(0)]^2 \rangle$, for $N = 2000$. The different scaling regimes are denoted by black bars.

For the GLJ data in Fig. 4(b) we observe for collapsed chains with $N \gtrsim 100$ a scaling exponent of $\alpha = 5/3$, which is in between the ideal limits of the SSS and WF scaling predictions and close to a recent analytical proposal [24]. While the generalized SSS scaling Eq. (7) predicts $\alpha = 1$ for a collapsed chain ($\nu_{\text{st}} = 1/3$), the generalized WF scaling Eq. (6) correctly gives $\alpha = \lambda = 5/3$ for a collapsed chain ($\nu_{\text{st}} = \nu_{\text{dyn}} \equiv 1/3$). The observed scaling can thus be interpreted as a generalization of the WF scaling.

Curiously, for $\nu_{\text{dyn}} = 1/3$ one would from Eq. (5) expect $\beta = 2/5$, in contrast to $\beta = 6/11$ (as follows using $\nu_{\text{dyn}} = 3/5$) seen in Figs. 3(d) and 5. On the other hand, the scaling of the chain relaxation time in Fig. 4(c) is rather consistent with the exponent $\lambda = 11/9$ which follows from Eq. (6) using $\nu_{\text{st}} = 1/3$ and $\nu_{\text{dyn}} = 3/5$. The difference of the exponents α and λ characterizing the cyclization time τ_{cyc} and the relaxation time τ_{rel} can be understood by considering the MSD of a terminal monomer of a $N = 2000$ GLJ chain, shown in the inset of Fig. 5, which exhibits three distinct scaling regimes: While for $t \lesssim 10^4$ ps the MSD displays swollen scaling, $\beta = 6/11$, for intermediate times $10^4 \text{ ps} \lesssim t \lesssim 10^6$ ps we observe collapsed scaling $\beta = 2/5$, until for longer times diffusive behavior $\beta = 1$ is found. We thus expect collapsed scaling to only become relevant on timescales $t \gtrsim 10^4$ ps, and indeed the cyclization times of the GLJ chains shown in Fig. 4(b) are of that order. The corresponding relaxation times in Fig. 4(c) on the other hand are slightly smaller, and thus still dominated by swollen statistics, characterized by the exponent $\lambda = 11/9$.

In conclusion, the cyclization dynamics of a slightly collapsed, self-avoiding chain is characterized by an exponent $\alpha = 5/3$ which is in between the classical SSS

and WF predictions of $3/2$ and 2 . Because a finite-length collapsed self-avoiding polymer exhibits a complex cross-over of swollen to collapsed behavior, the cyclization time scaling τ_{cyc} differs for finite chain lengths from the relaxation time scaling τ_{rel} . Our comprehensive picture of the cyclization crossover dynamics also applies to the dynamics of intrachain distances as probed in the collapsed globular state of proteins [50,51]. The generalized WF and SSS scalings given by Eqs. (6), (7) contain all scalings found in literature [2,3,21–25] and are expected to be independent of details of the chain interactions. Our explicit characterization of the non-Markovian dynamics of R_{ete} will be helpful in further understanding the first-passage distributions observed in cyclization of polypeptides [1,52,53]. In future work it will be interesting to study the effects of hydrodynamic interactions [40,54,55].

Funding by the DFG (Deutsche Forschungsgemeinschaft) via Grant No. SFB 1114/B02 is acknowledged.

-
- [1] L. Milanesi, J. P. Waltho, C. A. Hunter, D. J. Shaw, G. S. Beddard, G. D. Reid, S. Dev, and M. Volk, *Proc. Natl. Acad. Sci. U.S.A.* **109**, 19563 (2012).
- [2] L. J. Lapidus, W. A. Eaton, and J. Hofrichter, *Proc. Natl. Acad. Sci. U.S.A.* **97**, 7220 (2000).
- [3] O. Bieri, J. Wirz, B. Hellrung, M. Schutkowski, M. Drewello, and T. Kiefhaber, *Proc. Natl. Acad. Sci. U.S.A.* **96**, 9597 (1999).
- [4] A. Amitai and D. Holcman, *Phys. Rep.* **678**, 1 (2017).
- [5] H. Krämer, M. Niemöller, M. Amouyal, B. Revet, B. von Wilcken-Bergmann, and B. Müller-Hill, *EMBO J.* **6**, 1481 (1987).
- [6] S. Kadauke and G. A. Blobel, *Biochim. Biophys. Acta* **1789**, 17 (2009).
- [7] S. Holwerda and W. d. Laat, *Front. Genet.* **3**, 217 (2012).
- [8] G. Wilemski and M. Fixman, *J. Chem. Phys.* **58**, 4009 (1973).
- [9] G. Wilemski and M. Fixman, *J. Chem. Phys.* **60**, 866 (1974).
- [10] G. Wilemski and M. Fixman, *J. Chem. Phys.* **60**, 878 (1974).
- [11] M. Doi, *Chem. Phys.* **9**, 455 (1975).
- [12] A. Szabo, K. Schulten, and Z. Schulten, *J. Chem. Phys.* **72**, 4350 (1980).
- [13] I. M. Sokolov, *Phys. Rev. Lett.* **90**, 080601 (2003).
- [14] J. J. Portman, *J. Chem. Phys.* **118**, 2381 (2003).
- [15] T. Guérin, O. Bénichou, and R. Voituriez, *J. Chem. Phys.* **138**, 094908 (2013).
- [16] D. J. Bicout and A. Szabo, *J. Chem. Phys.* **106**, 10292 (1997).
- [17] T. Guérin, O. Bénichou, and R. Voituriez, *Nat. Chem.* **4**, 568 (2012).
- [18] R. W. Pastor, R. Zwanzig, and A. Szabo, *J. Chem. Phys.* **105**, 3878 (1996).
- [19] J. Z. Y. Chen, H.-K. Tsao, and Y.-J. Sheng, *Phys. Rev. E* **72**, 031804 (2005).
- [20] M. Sakata and M. Doi, *Polym. J.* **8**, 409 (1976).
- [21] L. J. Lapidus, P. J. Steinbach, W. A. Eaton, A. Szabo, and J. Hofrichter, *J. Phys. Chem. B* **106**, 11628 (2002).
- [22] N. M. Toan, D. Marenduzzo, P. R. Cook, and C. Micheletti, *Phys. Rev. Lett.* **97**, 178302 (2006).
- [23] A. Podtelezhnikov and A. Vologodskii, *Macromolecules* **30**, 6668 (1997).
- [24] P. Debnath and B. J. Cherayil, *J. Chem. Phys.* **120**, 2482 (2004).
- [25] F. Krieger, B. Fierz, O. Bieri, M. Drewello, and T. Kiefhaber, *J. Mol. Biol.* **332**, 265 (2003).
- [26] Z. Guo and D. Thirumalai, *Biopolymers* **36**, 83 (1995).
- [27] A. N. Rissanou, S. H. Anastasiadis, and I. A. Bitsanis, *J. Polym. Sci., Part B* **44**, 3651 (2006).
- [28] N. M. Toan, G. Morrison, C. Hyeon, and D. Thirumalai, *J. Phys. Chem. B* **112**, 6094 (2008).
- [29] D. Panja, *J. Stat. Mech.* (2010) L02001.
- [30] C. Maes and S. R. Thomas, *Phys. Rev. E* **87**, 022145 (2013).
- [31] H. Vandebroek and C. Vanderzande, *J. Stat. Phys.* **167**, 14 (2017).
- [32] P. Debnath, W. Min, X. S. Xie, and B. J. Cherayil, *J. Chem. Phys.* **123**, 204903 (2005).
- [33] M. J. Abraham, T. Murtola, R. Schulz, S. Páll, J. C. Smith, B. Hess, and E. Lindahl, *SoftwareX* **1–2**, 19 (2015).
- [34] C. Oostenbrink, A. Villa, A. E. Mark, and W. F. Van Gunsteren, *J. Comput. Chem.* **25**, 1656 (2004).
- [35] See Supplemental Material at <http://link.aps.org/supplemental/10.1103/PhysRevLett.122.067801> for details on numerical simulations and analytical calculations.
- [36] B. J. Berne and G. D. Harp, in *Advances in Chemical Physics* (John Wiley & Sons, Inc., Hoboken, NJ, 1970), Vol. 17, pp. 63–227.
- [37] J. O. Daldrop, J. Kappler, F. N. Brüning, and R. R. Netz, *Proc. Natl. Acad. Sci. U.S.A.* **115**, 5169 (2018).
- [38] R. Zwanzig, *Phys. Rev.* **124**, 983 (1961).
- [39] H. Mori, *Prog. Theor. Phys.* **33**, 423 (1965).
- [40] M. Doi and S. F. Edwards, *The Theory of Polymer Dynamics*, International Series of Monographs on Physics No. 73 (Clarendon Press, Oxford, 2007), oCLC: 845169495.
- [41] M. Rubinstein and R. H. Colby, *Polymer Physics (Chemistry)* (Oxford University Press, Oxford, 2003).
- [42] H. Hofmann, A. Soranno, A. Borgia, K. Gast, D. Nettels, and B. Schuler, *Proc. Natl. Acad. Sci. U.S.A.* **109**, 16155 (2012).
- [43] K. Kremer and K. Binder, *J. Chem. Phys.* **81**, 6381 (1984).
- [44] G. S. Grest and K. Kremer, *Phys. Rev. A* **33**, 3628 (1986).
- [45] J. C. F. Schulz, L. Schmidt, R. B. Best, J. Dzubiella, and R. R. Netz, *J. Am. Chem. Soc.* **134**, 6273 (2012).
- [46] M. K. Scherer, B. Trendelkamp-Schroer, F. Paul, G. Pérez-Hernández, M. Hoffmann, N. Plattner, C. Wehmeyer, J.-H. Prinz, and F. Noé, *J. Chem. Theory Comput.* **11**, 5525 (2015).
- [47] R. Morgado, F. A. Oliveira, G. G. Batrouni, and A. Hansen, *Phys. Rev. Lett.* **89**, 100601 (2002).
- [48] D. Ceperley, M. H. Kalos, and J. L. Lebowitz, *Phys. Rev. Lett.* **41**, 313 (1978).
- [49] P. G. De Gennes, *Macromolecules* **9**, 594 (1976).
- [50] S. C. Kou and X. S. Xie, *Phys. Rev. Lett.* **93**, 180603 (2004).
- [51] W. Min, G. Luo, B. J. Cherayil, S. C. Kou, and X. S. Xie, *Phys. Rev. Lett.* **94**, 198302 (2005).

- [52] J. Gowdy, M. Batchelor, I. Neelov, and E. Paci, *J. Phys. Chem. B* **121**, 9518 (2017).
- [53] M. Volk, Y. Kholodenko, H. S. M. Lu, E. A. Gooding, W. F. DeGrado, and R. M. Hochstrasser, *J. Phys. Chem. B* **101**, 8607 (1997).
- [54] E. P. Petrov, T. Ohrt, R. G. Winkler, and P. Schwille, *Phys. Rev. Lett.* **97**, 258101 (2006).
- [55] M. Hinczewski and R. R. Netz, *Macromolecules* **44**, 6972 (2011).